MIXED-SENSITIVITY $\mathscr{H}_\infty$ ON-BLADE CONTROL

Mr Jahaz Alotaibi
jhsa1@leicester.ac.uk, Dept. of Engineering, University of Leicester, Leicester, UK, LE1 7RH
Dr Rafael Morales
rmm23@leicester.ac.uk, Dept. of Engineering, University of Leicester, Leicester, UK, LE1 7RH

Abstract
In this work, we investigate the use of $\mathscr{H}_\infty$ control design for OBC. The designed methods are tested on a hingeless analytical rotor model of the four-blade Airbus EC-145 helicopter with Active Trailing Edge Flaps (ATEF). In order to enable the application of the control methods, system identification tools are applied to extract two-input two-output Linear-Time-Invariant models at hover, 20, 40, 60, 80 and 100 knots forward flight. Such linear approximations are obtained after the rotor is trimmed with zero trailing edge flapping. The vibration reduction strategy is developed using robust control mixed-sensitivity methods targeting the fixed-frame 4/rev vertical force component with 4/rev flaps. The strategy is shown to be satisfactory in the sense that vibration mitigation is obtained with the implementation of a *single* controller operating for all considered forward flight cases. The vibration reduction was 60% in average in terms of the 4/rev component of the vertical hub force and the vibration reduction scheme is not interfering with the trimming of the rotor.

NOMENCLATURE

R, a	=	blade radius and blade lift curve slope
c, c_f	=	blade and trailing-edge flap mean chord
m, M_h	=	blade and fuselage mass
e_β, e_ζ	=	blade flapping, lagging hinge offset
e_θ	=	pitch bearing offset
C_β, C_ζ	=	flapping and lagging damping constant
C_θ	=	pitching damping constant
K_β, K_ζ	=	flapping and lagging spring constant
K_θ	=	pitching spring constant
e_{air}	=	blade aerodynamic profile
Ω, ρ	=	rotor rotation speed, air density
C_{m_0}	=	blade profile moment coefficient
C_{d_2}	=	blade profile drag coefficient
C_{d_0}	=	blade profile drag mean coefficient
α_0, α_r	=	zero lift and rotor tilt angle
λ, μ	=	inflow and advance ratios
I_b	=	x and z moments of inertia of blade with respect to center of mass
I_θ	=	y (torsional) moment of inertia of blade with respect to center of mass
h	=	offset of rotor hub
$0, c, s$	=	collective, longitudinal and lateral cyclic
x_{aero}	=	x coordinate of blade aerodynamic center
ζ, β, θ	=	blade lagging, flapping and pitch angle
Θ, ψ	=	blade total pitch angle, blade azimuth angle
η, ϕ	=	trailing-edge flap deflection angle, inflow angle
ϑ	=	blade control pitch angle (rotor input)
q	=	vector of generalized coordinates
Q	=	vector of generalized forces
T, V	=	kinetic and potential energy

1. INTRODUCTION

Technologies for next-generation of helicopters explore embedding actuators in the blades of the main rotor in order to improve the performance in terms of reduced vibration, noise footprint and improved rotor efficiency. This stream of research known as On-Blade Control (OBC), has devoted its efforts to vibration reduction mainly[3]. On-blade Control (OBC) is an active control method which is currently being researched and tested by leading rotorcraft manufacturers and research centres across the globe[3]. Active trailing-edge flaps (ATEFs) are one form of OBC actuation, whereby flaps are located at the trailing-edge part of the blades providing deflection angles which affect the aerodynamic properties of the blade. The first step for designing an effective OBC helicopter vibration controller is the development of a representative model. The derivation of the main rotor behaviour is excruciatingly complex, even in cases where simplifying assumptions are made, such as rigid blades, no off-set hinges, no blade-tip aerodynamic losses and uniform inflow[5]. State-of-the-art numerical models target high levels of accuracy, thus compromising the simplicity and transparency of such models, and increasing the difficulty of extracting models fit for initial stages of control design. With this in mind, we develop the vibration reduction control strategy based on linear representations of the EC-145 rotor model with ATEFs developed by Maurice et al[7] for the following forward flight conditions. This model represents a hingeless rotor with offset hinges and limited stiffness and damping at the root of the blade. The model has been validated against the more comprehensive CAMRAD (Comprehensive Analytical Model of Rotorcraft Aerodynamics and Dynamics) II model and flight campaign data.

Most of the existing OBC algorithms are developed on the same principles of the more popular Higher Harmonic Control (HHC)[2,6], whereby the quasi-steady behaviour of the rotor process is assumed linear and static[4], and algorithms are constructed in the frequency domain to optimise the steady-state behaviour[8]. Our approach to attenuate helicopter vibration is to design $\mathscr{H}_\infty$ controllers using mixed-sensitivity methods. The methodology consist mainly on choosing weights to specify robustness measures, steady-state vibration reduction targets, convergence rate and control effort characteristics in the frequency domain. The motivation behind exploring the use of $\mathscr{H}_\infty$[9] for this application is two-fold: i) $\mathscr{H}_\infty$ methods offer the advantage that for a given Linear-Time-Invariant (LTI) model, which in this case is associated to the rotor vibration behaviour at each cruise condition, a controller which ensures a minimum level of performance can be obtained while also ensuring desired stability margins. The identified system, as explained later, is multi-variable with two inputs and two outputs, each of them associated with a cosine and sine coefficients for the ATEF deflection angles and the 4/rev vertical force component. Such properties are difficult to include at the design stage with more traditional HHC control approaches since the dynamics of the open-loop process and estimation filters are ignored and the strategy is mostly based on steady-state performance. ii) $\mathscr{H}_\infty$ control offers the benefit of handling dynamic couplings in a more transparent way between the chosen inputs and outputs.

The paper is organized as follows. First, the analytical hingeless helicopter rotor model will be briefly described in Section 2. Adequate open-loop input-output responses are recorded to then implement system identification tools to extract LTI models, with 4/rev trailing edge flaps defined as system inputs and the 4/rev vertical hub force components as outputs. Such a linear approximation task is explained in Section 3. After the linear models are identified, the paper proceeds to explain the main ideas behind the control design in Section 4 and also illustration of the results for both, under the linear representation and the analytical nonlinear model by Maurice et al[7]. The paper concludes with some final remarks in Section 5.

2. ANALYTICAL ROTOR MODEL

We provide a brief description on the implementation of the analytical model of the EC-145 main rotor to perform the control design task. The model is implemented by the main equations described in the paper of Maurice et al[7]. However, the integration of blade-element aerodynamic forces has been implemented in closed-form for increased computational efficiency and higher accuracy. Rotor characteristics are shown in Table 1.

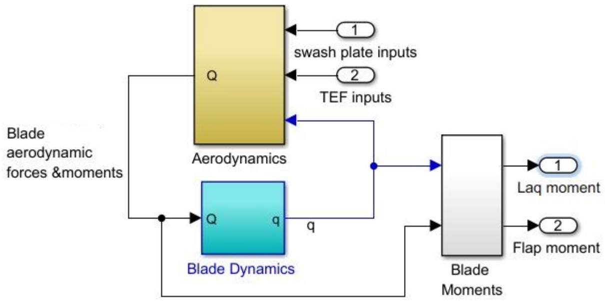

Figure 1: Overall structure of the single blade model

Table 1: Parameter of Helicopter model[7]

Parameter	Value	Unit	Parameter	Value	Unit
R	5.5	m	m	37	kg
R_1	$0.718R$	m	M_h	3000	kg
R_2	$0.827R$	m	K_β	20000	$N.m/rad$
e_β	0.65	m	C_β	0	$N.m.s/rad$
e_ζ	0.8	m	K_ζ	13000	$N.m/rad$
e_θ	0.8	m	C_ζ	280	$N.m.s/rad$
e_{air}	0.8	m	K_θ	5000	$N.m/rad$
y_c	$0.4R$	m	C_θ	4.75	$N.m.s/rad$
x_c	-0.038	m	I_b	71	$kg.m^2$
x_{aero}	-0.03	m	I_θ	0.25	$kg.m^2$
c	0.325	m	Ω	6.39	Hz
c_f	0.05	m	ρ	1.225	$kg.m^{-3}$
h	1.5	m	a	5.73	–
k_ζ	4	m	C_{d_0}	0.0079	–
k_β	1	m	C_{d_2}	0.4	–
g	9.81	ms^{-2}	C_{m_0}	-0.02	–

The model was built under Matlab and Simulink, which greatly facilitates the implementation of the controller in closed-loop[1]. The analytical model of the rotor is comprised of three major components: blade dynamics, aerodynamics and blade moments, see Fig. 1. Each of these subsystems are explained in more detail below.

2.1. Blade Dynamics

The equations of motion for a single blade are obtained via the Lagrangian approach. The generalised coordinates are chosen as the blade lag angle ζ, flap angle β and the pitch angle θ. The equations of motion are obtained[7] after working out the kinetic and potential energies for a single blade, leading to the following equations:

$$
\begin{aligned}
Q_{lag} &= [I_b + m(y_c - e_\zeta)^2 + mx_c^2]\ddot{\zeta} + C_\zeta\dot{\zeta} \\
&+ [K_\zeta + m(\Omega)^2 e_\zeta (y_c - e_\zeta)]\zeta \\
&- 2\Omega[I_b - I_\theta + m(y_c(y_c - e_\zeta - e_\beta) + e_\zeta e_\beta)]\beta\dot{\beta} \\
&+ [(I_\theta + mxc^2)\dot{\Theta} + 2m\Omega x_c(y_c - e_\zeta)]\dot{\beta} \\
&- m\Omega e_\zeta x_c \cos\Theta \\
&+ mx_c^2 \sin\Theta\cos\Theta(\ddot{\beta} - \Omega^2\dot{\beta} - 2\Omega\dot{\Theta}) \\
&+ mx_c(y_c - e_\zeta)\ddot{\Theta}\sin\Theta
\end{aligned} \tag{1}
$$

$$
\begin{aligned}
Q_{flap} &= [I_b + m(y_c - e_\beta)^2]\ddot{\beta} + C_\beta\dot{\beta} \\
&+ [K_\beta + \Omega^2(I_b - I_\theta + my_c(y_c - e_\beta))]\beta - K_\beta\beta_\rho \\
&+ 2\Omega[I_b - I_\theta + m(y_c(y_c - e_\zeta - e_\beta) + e_\zeta e_\beta)]\beta\dot{\zeta} \\
&- [m(y_c - e_\beta)x_c\cos\Theta + (I_\theta + mx_c^2)\zeta]\ddot{\Theta} \\
&- [\Omega(I_\theta + mx_c^2(1 - \cos(2\Theta))) + ((I_\theta + mx_c^2))\dot{\zeta} \\
&+ mx_c^2\Omega]\dot{\Theta} - (m\Omega^2 y_c x_c)\sin\Theta \\
&- 2m\Omega x_c(y_c - e_\zeta)\dot{\zeta}\sin\Theta \\
&+ (mx_c^2)(\ddot{\zeta} - \Omega^2\zeta)\cos\Theta\sin\Theta
\end{aligned} \tag{2}
$$

$$
\begin{aligned}
Q_{pitch} &= (I_\theta + mx_c^2)\ddot{\Theta} + C_\theta\dot{\theta} + K_\theta\theta \\
&+ (I_\theta + mx_c^2)(\Omega - \dot{\zeta})\dot{\beta} - (m(y_c - e_\beta)x_c)\ddot{\beta}\cos\Theta \\
&+ (mx_c(y_c - e_\zeta)\ddot{\zeta}\sin\Theta + \frac{mx_c^2\Omega^2}{2}\sin(2\Theta) \\
&- m\Omega^2 x_c(y_c\beta\cos\Theta - e_\zeta\zeta\sin\Theta) \\
&- \dot{\beta}\zeta(I_\theta + mx_c^2) + mx_c^2\Omega(\dot{\zeta}\sin(2\Theta) - \dot{\beta}\cos(2\Theta))
\end{aligned} \tag{3}
$$

$Q^T = [Q_{lag}, Q_{flap}, Q_{pitch}]$ is the vector of generalized forces modelling the aerodynamic loads acting on the blade and the total pitch angle is expressed as $\Theta = \theta + \vartheta$, with ϑ denoting the swashplate input.

2.2. Aerodynamics

The generalised forces are constructed by integrating elementary aerodynamic forces across the radial direction for a single blade

$$
\begin{bmatrix} Q_{lag} \\ Q_{flap} \\ Q_{pitch} \end{bmatrix} \simeq \int_{e_{air}}^{R} \begin{bmatrix} -(r - e_\zeta)dF_x + x_{aero}dF_r \\ (r - e_\beta)dF_z + x_{aero}(\Theta dF_r + \zeta dF_z) \\ dM_\theta - x_{aero}(dF_z + \Theta dF_x) \end{bmatrix} dr \tag{4}
$$

For a given blade element, an elementary lift dL is normal to the blade section airflow velocity, the drag dD is tangential to the blade section airflow velocity, and the radial force dF_r is in the direction along the blade. The feathering moment is indicated by dM_θ. The blade element aerodynamic forces are defined with respect to the blade-section velocity axes and must, therefore, be projected on the lagging frame with the inflow angle ϕ. The aerodynamic forces act at the aerodynamic centre, and the pitching moment is assumed to be around the blade feathering axis. For more information, refer to the paper by MAurice et al[7].

The integration of the generalized forces have been implemented analytically to increase the computational efficiency and the accuracy of the model, see equations (5, 6 and 7). The final expressions are polynomial functions in terms of R and e_{air} with time-varying coefficients.

$$
\begin{aligned}
Q_{flap} &= S_7(\frac{R^4}{4} - \frac{e_{air}^4}{4}) + (S_8 + S_{11})(\frac{R^3}{3} - \frac{e_{air}^3}{3}) \\
&+ (S_9 + S_{12})(\frac{R^2}{2} - \frac{e_{air}^2}{2}) + (S_{13} - S_{10})(R - e_{air})
\end{aligned} \tag{5}
$$

$$
\begin{aligned}
Q_{lag} &= -S_1(\frac{R^4}{4} - \frac{e_{air}^4}{4}) \\
&+ (S_4 + (e_\zeta S_1 - S_2))(\frac{R^3}{3} - \frac{e_{air}^3}{3}) \\
&+ (S_5 + (e_\zeta S_2 - S_3))(\frac{R^2}{2} - \frac{e_{air}^2}{2}) \\
&+ (S_6 + (e_\zeta S_3)(R - e_{air})
\end{aligned} \tag{6}
$$

$$
\begin{aligned}
Q_{pitch} &= S_{14}(\frac{R^3}{3} - \frac{e_{air}^3}{3}) + S_{15}(\frac{R^2}{2} - \frac{e_{air}^2}{2}) \\
&+ S_{16}(R - e_{air})
\end{aligned} \tag{7}
$$

For the expressions of all the terms $S_1, ..., S_{16}$, please refer to the paper[1].

2.3. Blade Moments

Blade pitch and lag moments are denoted as M_β and M_ζ, respectively. Theses blade moments result from the aerodynamic forces F_x and F_z action on the aerodynamic center, the forces arising from the acceleration of the center of mass and the moments arising from the hinge springs and dampers. The measured equations can be written by using Newton's second law[7] as:

$$M_\zeta = k_\zeta(m\zeta_{a(O_{cg})}.x_\zeta - F_x) - K_\zeta\zeta - C_\zeta\dot{\zeta} \tag{8}$$

$$M_\beta = k_\beta(F_z - m\beta_{a(O_{cg})}.z_\beta) - K_\beta(\beta - \beta_\rho) - C_\beta\dot{\beta} \tag{9}$$

Finally, we integrate the three subsystems (dynamics, aerodynamics and blade moments) to generate the single blade model. The single blade MIMO model is then generalised for the remaining three blades to generate the four blade model, by assuming all the blades are identical and undergo identical motion but at a different azimuth angle.

3. LINEARISATION

For vibration reduction, we are interested in reducing the vertical component of the rotor thrust F_z. The net vertical force for each blade is obtained as shown in the paper by Maurice et al:

$$Fz_i = \frac{\rho ac}{2}\left(F + \eta_i\left[\frac{K_4 c_f}{ac} - K1\right]G_f\right), i = 1, ...4 \tag{10}$$

F_z is then obtained as the sum of all contributions of Fz_i for all blades, where i denotes the blade index

$$F_z = \sum_i Fz_i$$

The rotor thrust F_z can also be obtained from the vertical shear force obtained for each blade at its root, however this approach was not pursued here. Because F_z is periodic, it can be expressed as a Fourier series

$$F_z = Fz_0 + \sum_{n=1}^{\infty} Fz_{nc}\cos(n\psi) + Fz_{ns}\sin(n\psi) \tag{11}$$

with the outputs being the 4/rev components Fz_{4c} and Fz_{4s}. In terms of the inputs to the system, we focus on the 4/rev components of the ATEF deflection angles. For the first (reference) blade, its deflection angle can be described as

$$\eta_1(\psi) = \eta_{4c}(t)\cos(4\psi) + \eta_{4s}(t)\sin(4\psi) \tag{12}$$

with $\eta_{4c}(t)$ and $\eta_{4s}(t)$ being the inputs to the system. The linearisation tasks consists in modelling the relation between these sets of inputs and outputs by a trasnfer function matrix.

The above set of inputs and outputs were chosen following well-known results from rotor vibration theory, which predicts that 4/rev blade shear forces translate to 4/rev components of the vertical hub force for a four-blade rotor under the assumptions that all blades undergo identical motion. Initial experiments in open loop corroborated this fact, showing that 4/rev ATEF components were decoupled from the bias vertical hub force component Fz_0. This is particularly beneficial because such inputs are desired not to interfere with the trimming of the rotor or the flight control mechanism. Another method followed for linearisation uses Multi-blade Coordinates (MBC) transformations[5]. This approach would be valid as long as inthis case the rotor thrust expressed in the fixed-frame is comprised mainly by a first harmonic expression. The advantage of this approach is that the dynamics of the MBC coefficients in the fixed frame can also be expressed by Linear Time-Invariant differential equations for valid cases. However, after open-loop experiments, this was not the case for the hub vertical force and therefore this approach was not followed. The response of cosine and sine elements of Fz in MBC in the fixed-frame coefficients were highly oscillatory (not constant), suggesting that their dynamics can not be captured by a LTI equation.

Th linearisation was obtained from using system identification tools in Matlab. The results for the considered forward flight cases are shown in Figures 2 - 7. The inputs in these graphs u_1 and u_2 correspond to η_{4c} and η_{4s}, respectively. Similarly, the outputs shown as y_1 and y_2 correspond to Fz_{4c} and Fz_{4s}, respectively, and being unbiased. For each flight condition, one-degree amplitude step signals were inputted on each control input at a time after the rotor was being trimmed. The responses show a high gain in the sense that one degree flapping produces a change in the 4/rev vertical component between 4000 N and 6000 N. Swashplate inputs for trimming the rotor at each forward speed were obtained from the results in the paper by Maurice et al[7]. Step signals as shown in each of the graphs were applied and the response was recorded. This was repeated for each input separately. Each of the elements of the transfer function was obtained using the system identification tool (tfest) with order 4. As shown in the results for all conditions, the match provided by the system ID tool was excellent, with the responses from the transfer func-

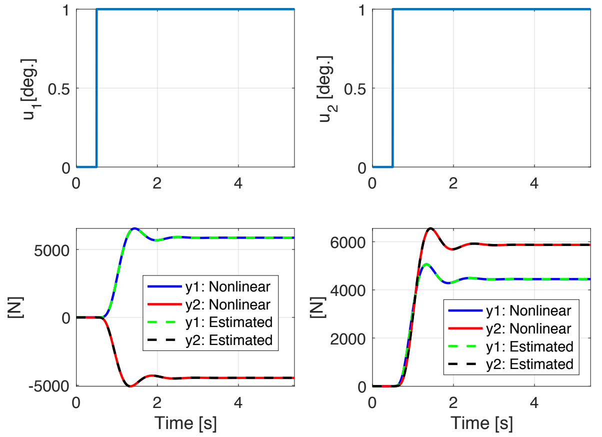

Figure 2: Linearization results for hover.

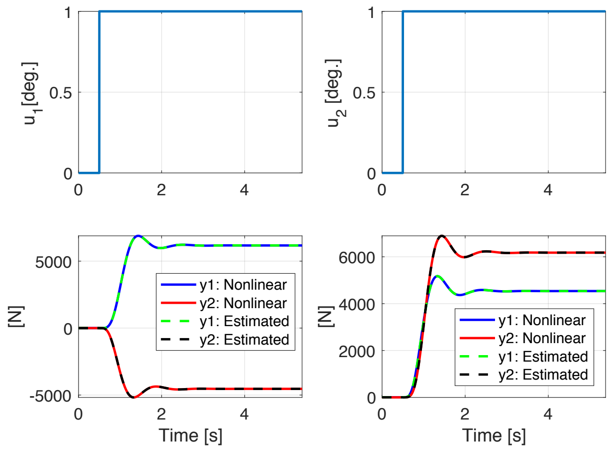

Figure 3: Linearization results at 20 knots.

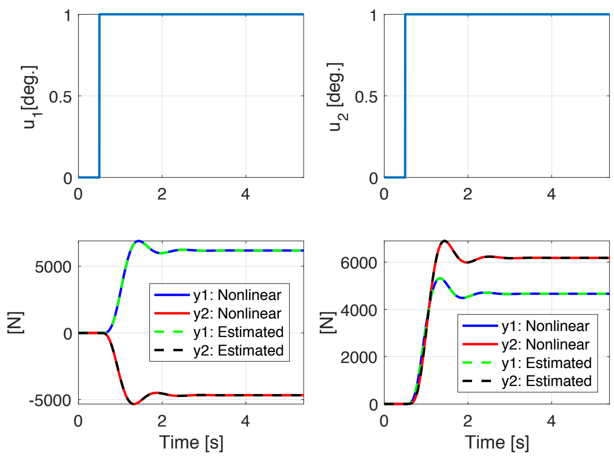

Figure 4: Linearization results at 40 knots.

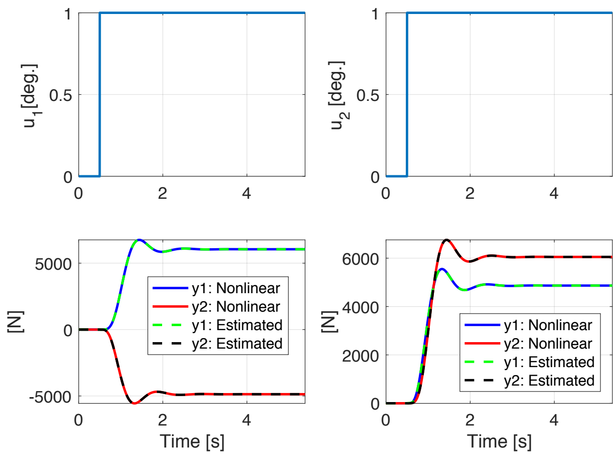

Figure 5: Linearization results at 60 knots.

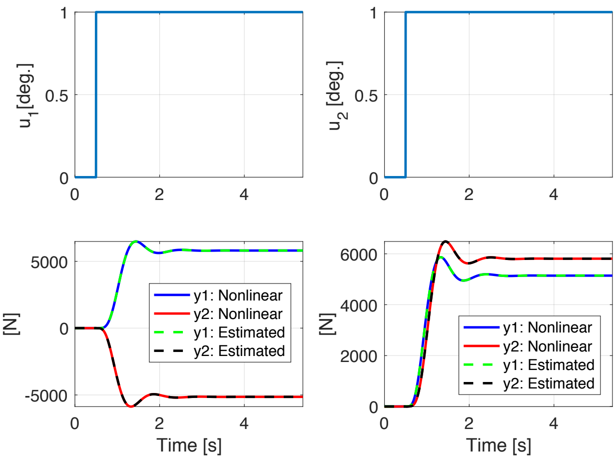

Figure 6: Linearization results at 80 knots.

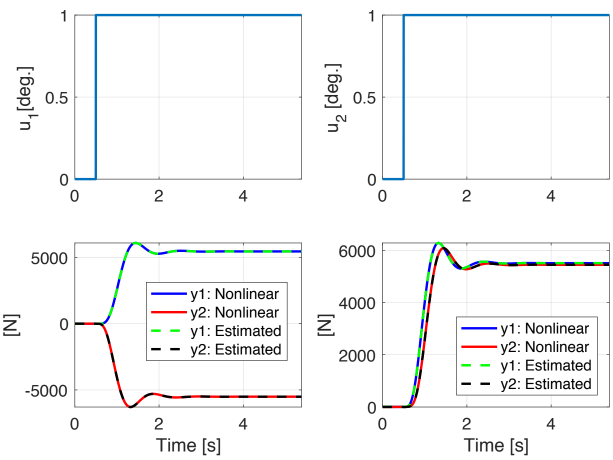

Figure 7: Linearization results at 100 knots.

tion matrix being almost identical to those by the nonlinear analytical model. Finally, the frequency response of all identified transfer function matrices are shown in Figure 8, all showing a bandwidth less than 10 rad/s, and

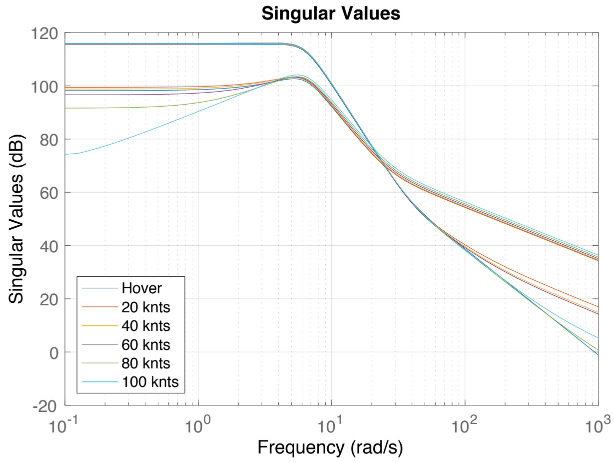

Figure 8: Singular values for all identified transfer function models.

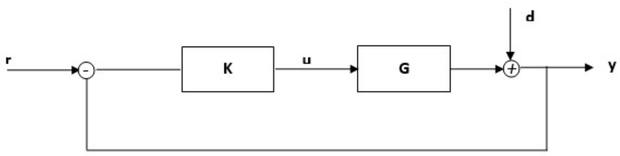

Figure 9: Classical feedback configuration

the 100 knots case being significantly different from the rest and showing a more pronounced peak amplitude around the bandwidth frequency. All identified models are stable with associated damping between 0.387 and 0.98 and time constant between 0.121 s and 0.41 s.

4. MIXED-SENSITIVITY $\mathscr{H}_\infty$ CONTROL DESIGN AND SIMULATION RESULTS

Our approach to attenuate helicopter vibration is to design $\mathscr{H}_\infty$ controllers using mixed-sensitivity methods[9]. The conventional feedback interconnection is shown in Figure 9, whereby the controller $K(s)$ is the designed LTI element to attenuate rotor vibrations and the plant G represent the rotor behaviour. When the behaviour is linearised, it can be represented in the Laplace domain as a transfer function matrix $G(s)$. The signal $d(t)$ accounts for the baseline vibration coefficients. In a control theory context, our design approach is to achieve a satisfactory level of *disturbance rejection*, i.e., to reduce the sensitivity of the baseline vibration $d(t)$ on the output signal $y(t)$. The control effrorts are denoted by u, which in our case refer to the 4/rev components of the ATEF deflection angles. The reference signal is denoted by $r(t)$, which in this case is set to zero as these are the target values for the outputs after closing the loop. The controller is designed first based on the models obtained from the linearisation section. Once a controller is obtained, which provides satisfactory level of robustness and performance under linear simulations, the controller is implemented on the nonlinear analytical model for a better

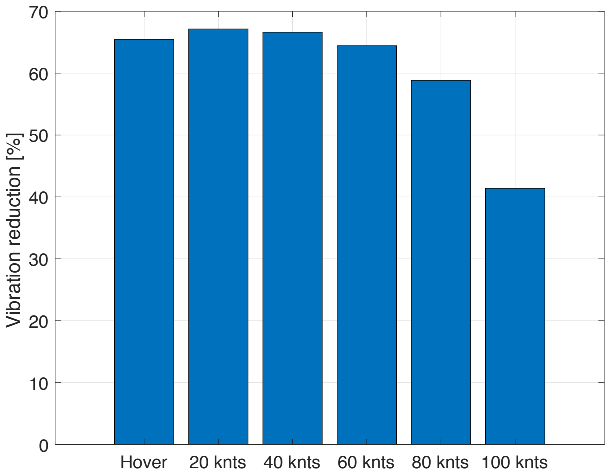

Figure 10: Vibration results for linear simulations.

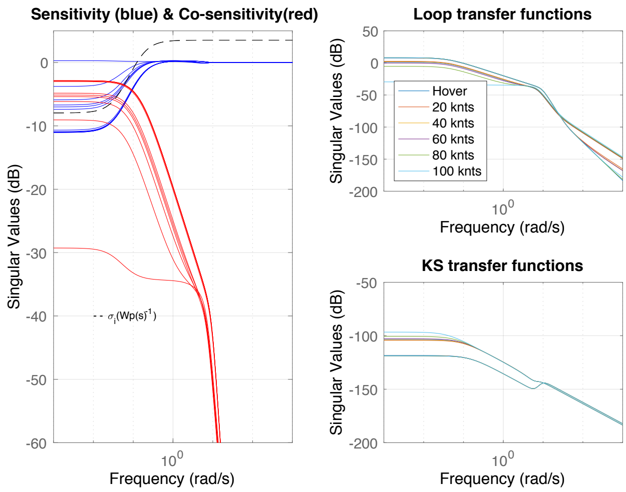

Figure 11: Linear results in the frequency domain.

assessment of the performance. Typically the controller is required to be finely retuned after this to achieve improved results with the nonlinear rotor model.

The mixed-sensitivity design approach is based on shaping two key closed-loop sensitivities transfer functions $S(s) = (I - G(s)K(s))^{-1}$ and $K(s)S(s)$. The shaping takes place in the frequency domain. The sensitivity is particularly important as it contains the information in terms of vibration reduction levels at steady-state, convergence rate and robustness. The shaping of $K(s)S(s)$ is included to account for the magnitude of the ATEF deflection angles used when performing the control taks. The mixed sensitivity problem can be solved by finding stabilizing controllers $K(s)$ such that the following norm is minimised[9]

$$\left\| \begin{bmatrix} W_p S \\ W_u KS \end{bmatrix} \right\|_\infty \tag{13}$$

The weights $W_p(s)$ and $W_u(s)$ are used to shape the sensitivity transfer function $S(s)$ and the control efforts $K(s)S(s)$, respectively. For the present case, we choose a diagonal $W_p(s)$ with the diagonal elements expressed as

$$W_{pi}(s) = \frac{s/M_i + \omega_{B_i}}{s + \omega_{B_i} A_i} \tag{14}$$

The parameters M_i, ω_{B_i} and A_i are chosen to specify robustness, closed-loop bandwidth (which translate in convergence rate in the time domain) and steady-state performance levels, respectively. The index i is used to the diagonal element. The weight $W_u(s)$ was chosen as a constant 2×2 matrix. Refer to Skogestad and Postlethwaite[9] for more details.

4.1. Linear results

We investigate the use of the model for control design. We concentrate the control design effort at the flying condition of at hover, 20, 40, 60, 80 and 100 knots in constant forward flight (cruise). The efforts were concentrated in finding a unique controller able to provide vibration reduction for all flight conditions. This is de-

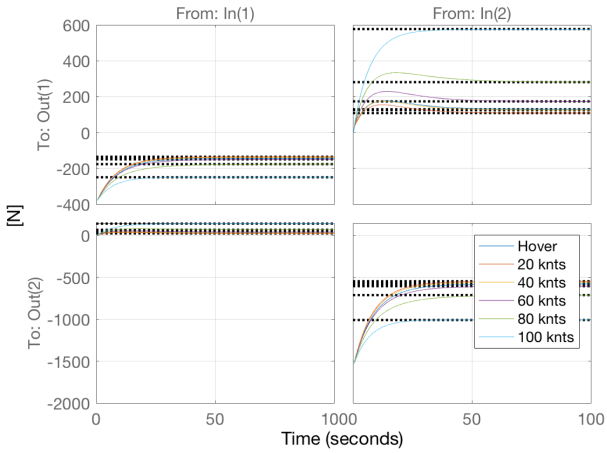

Figure 12: Output responses under linear simulations.

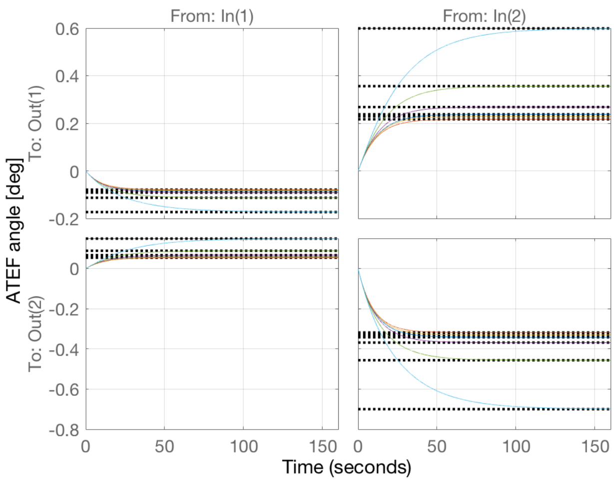

Figure 13: ATEF responses under linear simulations

sirable to reduce processing power and implementation demands. The controller was designed based on the linearised plant at 60 knots. A stabilising controller with order 17 was obtained. Frequency and time-domain results are shown in Figures 10-13. The design results are satisfactory in the sense that vibration reduction was achieved for all flight conditions with a single controller. Vibration reduction on the 4/rev component vary between 40% and 65%. The controller was obtained after choosing the same values for both diagonal elements of $W_p(s)$, with $\omega_{B_i} = 0.1$ rad/s, $M_i = 1.5$ and $A_i = 0.4$ and $W_u(s) = 1 \times 10^5 I$. Linear results in the frequency domain show also the singular values for th loop transfer functions $L(s) = G(s)K(s)$ and the co-sensitivity $T(s) = I - S(s)$. Step responses show both the time response of the outputs and also the ATEF deflection angles when a step signals in the output disturbance is applied separately, with an amplitude about 10% of the baseline value.

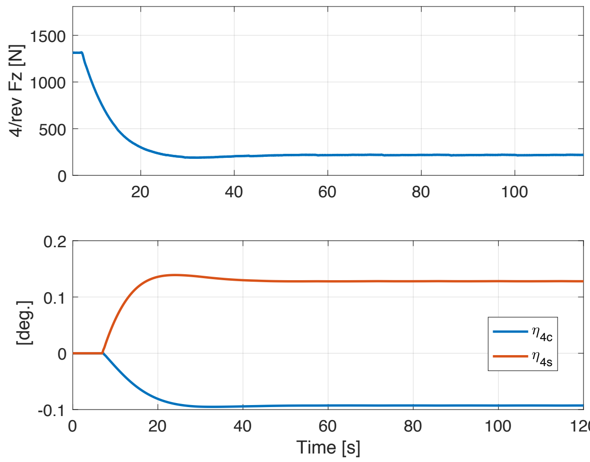

Figure 14: Closed-loop response at 100 knots case with nonlinear analytical rotor model

4.2. Nonlinear Results

The linear controller designed in the previous subsection was implemented on the nonlinear analytical rotor model in closed loop. The average values is about 60% for all flight conditions. Simulations were run so at the beginning the rotor is trimmed first and then the closed-loop controller is engaged after 7 s. The performance was satisfactory in the sense that achieved vibration reduction level were even better than those expected from linear results. In addition, it is was observed that the vibration control scheme is not interfering with the trimming of the rotor, with the blade coordinates (flap, lag and pitch) being practically the same after the controller is engaged. ATEF deflection angles were very small, in the order of tenths of degrees, due to the high sensitivity on the 4/rev component of the thrust to 4/rev components of the ATEF. Results are shown for the 100 knots flight condition, with Figure15 showing the evolution of the vertical hub load and Figure14 displaying the 4/rev component of F_z and 4/rev component of the ATEF deflection angles (control actions).

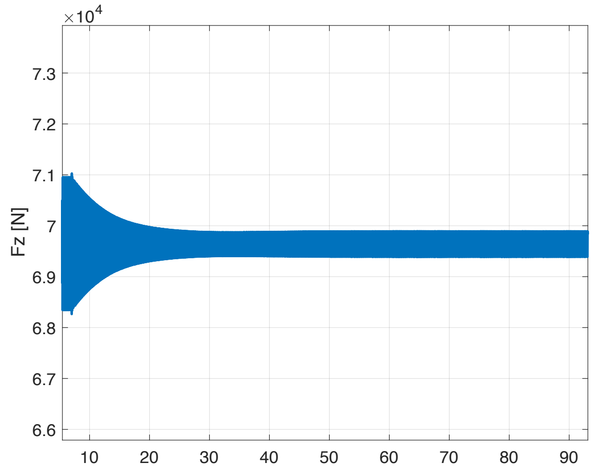

Figure 15: $F_z(t)$: Closed-loop response at 100 knots case with nonlinear analytical rotor model

5. CONCLUSIONS

This paper has described the methodology of using $\mathscr{H}_\infty$ control design for OBC. The overall results were highly satisfactory in the sense that significant reduction levels were achieved on the 4/rev rotor hub vertical force for several forward flight conditions. The control strategy was found not to interfere or modify the trimming of the rotor. Future work will explore on expanding the current approach to a more comprehensive one with taking into account the remaining hub loads and moments and achieve a desired trade off across the signals in terms of vibrating reduction.

REFERENCES

[1] J. Alotaibi and R. Morales. Efficient Implementation of a Helicopter Hingless Rotor Model with Active Trailing Edge Flaps for Control Design. In *12th UKACC International Conference on Control*, Sheffield, UK, 2018.

[2] F. H. Fan and S. R. Hall. Gain-Scheduled Higher Harmonic Control for Full Flight Envelope Vibration Reduction. In *Proceedings of the 70th American Helicopter Society Annual Forum*, 2014.

[3] P. P. Friedmann. On-blade control of rotor vibration, noise and performance: Just around the corner? *Journal of the American Helicopter Society*, 59:041001 (1–37), 2014.

[4] W. Johnson. Self-tuning regulators for multicyclic control of helicopter vibration. Technical Report NASA TP-1996, NASA, 1982.

[5] W. Johnson. *Rotorcraft Aeromechanics*. Cambridge Aerospace Series. Cambridge University Press, 2013.

[6] C. Kessler. Active rotor control for helicopters: motivation and survey on higher harmonic control. *CEAS Aeronautical Journal*, 1(1-4):23–54, 2011.

[7] J.-B. Maurice, F. A. King, and W. Fitcher. Derivation and validation of a helicopter rotor model with trailing-edge flaps. *Journal of Guidance, Control, and Dynamics*, 36(5):1375–1387, 2013.

[8] D. Patt, L. Liu, J. Chandrasekar, D. S. Bernstein, and P. P. Friedmann. HHC algorithm for helicopter vibration reduction revisited. *Journal of Guidance, Control and Dynamics*, 28(5):918 – 930, 2005.

[9] S. Skogestad and I. Postlethwaite. *Multivariable Feedback Control: Analysis and Design (second edition)*. John Wiley & Sons, 2005.